Health Physics Pergamon Press 1976. Vol. 31 (August), pp. 97–108. Printed in Northern Ireland

ENERGY ABSORPTION PATTERNS IN CIRCULAR TRIPLE-LAYERED TISSUE CYLINDERS EXPOSED TO PLANE WAVE SOURCES

HENRY S. HO

U.S. Department of Health, Education and Welfare, Public Health Service,
Food and Drug Administration, Bureau of Radiological Health,
Division of Biological Effects, 5600 Fishers Lane, Rockville, MD 20852

(*Received* 3 *November* 1975; *accepted* 30 *December* 1975)

Abstract—The energy absorption patterns in two sizes of triple-layered phantom tissue circular cylinders are calculated for plane wave sources of 433, 750, 918 and 2450 MHz. The result indicates that the energy absorption can be highly non-uniform and varies according to the size of the cylinder and the frequency of the source. It is concluded that energy absorption characterization in biological effects experiments must be considered if the results of these experiments were to be meaningful to radiation protection. In addition, energy penetration and absorption characteristics in tissues should be considered in the design of effective therapeutic heating apparatus.

INTRODUCTION

CURRENT microwave biological effects research uses various sizes of animals and cell cultures. Many experiments are conducted in plane wave exposure fields and quantified dosimetrically in terms of external field measurements presented in terms of power density (mW/cm^2). Biological effects, however, are more closely related to the induced internal electromagnetic fields in the biological body than to the exposure field. It is therefore important to determine the extent to which energy absorption is dependent on the size and shape of the biological body and the frequency of the irradiation source.

In the area of microwave therapeutic heating instrumentation design, the selection of diathermy frequencies and applicators for desired tissue heating characteristics may depend on the energy absorption characteristics in various shapes and sizes of body tissues.

In this theoretical investigation, the electromagnetic field inside a plane wave irradiated triple-layered dielectric cylinder is formulated. Using this formulation, a computer program is written to calculate the energy absorption pattern in two sizes of triple-layered tissue cylinders exposed to separate plane wave sources of 433, 750, 918 and 2450 MHz frequencies. The dielectric properties of bone, muscle, and fat tissues similar to those reported by Schwan *et al.* (Sc54) are used in the calculation.

FORMULATION OF THE PROBLEM

The general formulation of field patterns in circular dielectric cylinders due to plane wave sources has been reported by Wait (Wa55). By using the method of summation of cylindrical waves and matching of tangential fields across the boundaries, the field and hence heating patterns in a triple-layered dielectric cylinder due to plane wave sources can be computed.

Consider Fig. 1. An infinitely long triple-layered circular dielectric cylinder, with radii r_f, r_m, and r_b; and corresponding dielectric constants of ε_f, ε_m, and ε_b, simulates layers of fat, muscle, and bone tissues. Values of ε_f, ε_m, and ε_b are listed in Table 1.

A plane wave at normal incident on the dielectric cylinder is represented by

$$\psi_i = \exp[jk_0 r\cos(\phi)] = \sum_{n=-\infty}^{\infty} [j^n J_n(k_0 r)\exp(jn\phi)] \quad (1)$$

1

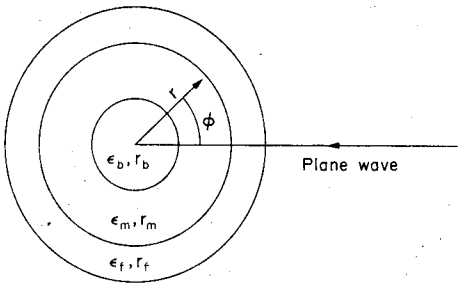

FIG. 1. Plane wave incident on triple-layered dielectric cylinder r_b, r_m, r_f and ε_b, ε_m, ε_f are respectively the radii and complex dielectric constants of bone, muscle and fat tissue layers.

where $\psi_i = E_z$ stands for E_z polarized (TM) wave, while $\psi_i = H_z$ stands for H_z polarized (TE) wave. **z** is along the axial direction of the dielectric cylinder. $k_0 = 2\pi/\lambda$ = wave number in free space. The scattered field is represented by

$$\psi_s = \sum_{n=-\infty}^{\infty} [C_n H_n^{(2)}(k_0 r) \exp(jn\phi)] \qquad (2)$$

where C_n are constants to be determined, and $H_n^{(2)}$ is the Hankel function of the second kind.

The fields in the dielectric layers obey the wave equation

$$(\nabla_t^2 + k^2)\psi = 0 \qquad (3)$$

where the subscript t denotes transverse (to z) operation, and k represents the wave number in the dielectric medium. Therefore the fields in the dielectric layers can be represented by

$$\psi_b = \sum_{n=-\infty}^{\infty} [A_{nb} J_n(k_b r) \exp(jn\phi)] \qquad (4)$$

$$\psi_m = \sum_{n=-\infty}^{\infty} [A_{nm} J_n(k_m r) + B_{nm} Y_n(k_m r)] \exp(jn\phi) \qquad (5)$$

$$\psi_f = \sum_{n=-\infty}^{\infty} [A_{nf} J_n(k_f r) + B_{nf} Y_n(k_f r)] \exp(jn\phi) \qquad (6)$$

$$k_b = k_0\sqrt{\varepsilon_b}$$
$$k_m = k_0\sqrt{\varepsilon_m} \qquad (7)$$
$$k_f = k_0\sqrt{\varepsilon_f}.$$

J_n, Y_n are respectively the Bessel functions of the first and second kind. The coefficients A_{nb}, A_{nm}, B_{nm}, A_{nf}, and B_{nf} are constants to be determined by the boundary conditions.

Table 1. Complex dielectric constants of tissues vs frequency

Frequency	Fat and Bone		Muscle	
MHz	$\varepsilon'_{f,b}$	$\varepsilon''_{f,b}$	ε'_m	ε''_m
27	20.00	10.16	108.0	377.5
433	5.61	1.96	52.8	47.4
750	5.61	1.45	51.5	30.2
918	5.61	1.31	51.4	25.2
1500	5.48	0.99	49.4	17.5
2450	5.48	0.86	47.3	16.2

$\varepsilon'_{f,b}$ Real part of dielectric constant, fat and bone.

$\varepsilon''_{f,b}$ Imaginary part of dielectric constant, fat and bone.

ε'_m Real part of dielectric constant, muscle.

ε''_m Imaginary part of dielectric constant, muscle.

BOUNDARY CONDITIONS E_z POLARIZED (TM) WAVE

$\psi_i = E_z$ for the E_z polarized (TM) wave. The tangential fields are E_z and H_ϕ, where

$$H_\phi = (1/j\omega\mu)\,\partial E_z/\partial r. \qquad (8)$$

The boundary conditions are:

$$E_{zi} + E_{zs} = E_{zf} \quad (\text{at } r = r_f) \qquad (9)$$
$$H_{\phi i} + H_{\phi s} = H_{\phi f} \quad (\text{at } r = r_f) \qquad (10)$$
$$E_{zf} = E_{zm} \quad (\text{at } r = r_m) \qquad (11)$$
$$H_{\phi f} = H_{\phi m} \quad (\text{at } r = r_m) \qquad (12)$$
$$E_{zm} = E_{zb} \quad (\text{at } r = r_b) \qquad (13)$$
$$H_{\phi m} = H_{\phi b} \quad (\text{at } r = r_b) \qquad (14)$$

where the subscripts i and s denote respectively the incident and the scattered field, while, the subscripts f, m, and b denote the media fat, muscle and bone.

Using the equations (1)–(5) and (8)–(14), the coefficients of each cylindrical wave (with index n) can be expressed as a set of six simultaneous equations.

$$A_{nf}J_n(k_f r_f) + B_{nf}Y_n(k_f r_f) = j^n J_n(k_0 r_f) + C_n H_n^{(2)}(k_0 r_f) \qquad (15)$$

$$A_{nf}J_n'(k_f r_f) + B_{nf}Y_n'(k_f r_f) = (k_0/k_f)[j^n J_n'(k_0 r_f) + C_n H_n'^{(2)}(k_0 r_f)] \qquad (16)$$

$$A_{nm}J_n(k_m r_m)+B_{nm}Y_n(k_m r_m) = A_{nf}J_n(k_f r_m)+B_{nf}Y_n(k_f r_m) \quad (17)$$

$$A_{nm}J_n'(k_m r_m)+B_{nm}Y_n'(k_m r_m) = (k_f/k_m)[A_{nf}J_n'(k_f r_m)+B_{nf}Y_n'(k_f r_m)] \quad (18)$$

$$A_{nb}J_n(k_b r_b) = A_{nm}J_n(k_m r_b)+B_{nm}Y_n(k_m r_b) \quad (19)$$

$$A_{nb}J_n'(k_b r_b) = (k_m/k_b)[A_{nm}J_n'(k_m r_b)+B_{nm}Y_n'(k_m r_b)] \quad (20)$$

for integer n, $-\infty \le n \le \infty$. J_n', Y_n' and H_n' are respectively the derivatives of J_n, Y_n and H_n.

Using the six simultaneous equations of (15)–(20), the coefficients C_n, A_{nf}, B_{nf}, A_{nm}, B_{nm}, and A_{nb} can be found for all integer n. The field patterns in the dielectric layers can then be found. The absorbed power density (based on volume) (Jo73) in the dielectric medium is related to the electric field strength by the relationship:

$$P = \tfrac{1}{2}\sigma |E|^2 = \tfrac{1}{2}\omega\varepsilon'' |E|^2. \quad (21)$$

For the E_z polarized (TM) case, $\psi = E_z$. Therefore the

$$P = \tfrac{1}{2}\omega\varepsilon'' |\psi|^2 \quad (22)$$

where $\omega = 2\pi f$, f is the frequency of the plane wave, and ε'' is the imaginary part of the dielectric constant of the medium.

BOUNDARY CONDITIONS FOR H_Z POLARIZED (TE) WAVE

For H_z polarized (TE) wave, $\psi_i = H_z$. The tangential fields are H_z and E_ϕ, where

$$E_\phi = -(1/j\omega\varepsilon)\,\partial H_z/\partial r. \quad (23)$$

Using the continuity of the tangential electric and magnetic fields at r_f, r_m and r_b, the following set of six simultaneous equations can be obtained for each cylindrical wave.

$$A_{nf}J_n(k_f r_f)+B_{nf}Y_n(k_f r_f) = j^n J_n(k_0 r_f)+C_n H_n^{(2)}(k_0 r_f) \quad (24)$$

$$A_{nf}J_n'(k_f r_f)+B_{nf}Y_n'(k_f r_f) = (k_f/k_0)[j^n J_n'(k_0 r_f)+C_n H_n'^{(2)}(k_0 r_f)] \quad (25)$$

$$A_{nm}J_n(k_m r_m)+B_{nm}Y_n(k_m r_m) = A_{nf}J_n(k_f r_m)+B_{nf}Y_n(k_f r_m) \quad (26)$$

$$A_{nm}J_n'(k_m r_m)+B_{nm}Y_n'(k_m r_m) = (k_m/k_f)[A_{nf}J_n'(k_f r_m)+B_{nf}Y_n'(k_f r_m)] \quad (27)$$

$$A_{nb}J_n(k_b r_b) = A_{nm}J_n(k_m r_b)+B_{nm}Y_n(k_m r_b) \quad (28)$$

$$A_{nb}J_n'(k_b r_b) = (k_b/k_m)[A_{nm}J_n'(k_m r_b)+B_{nm}Y_n'(k_m r_b)] \quad (29)$$

for integer n, $-\infty \le n \le \infty$.

J_n', Y_n' and $H_n'^{(2)}$ are respectively the derivatives of J_n, Y_n and $H_n^{(2)}$.

Solving the simultaneous equations, the magnetic field in the dielectric cylinder is obtained. The absorbed power density (by volume) is related to the electric field strength by equation (21). For the H_z polarized (TE) case, $\psi = H_z$. Hence using Maxwell's equations,

$$\mathbf{E} = (1/j\omega\varepsilon)\nabla_t \times H_z\mathbf{z} = (1/j\omega\varepsilon)[(1/r)\,\partial H_z/\partial\phi\,\mathbf{r} - \partial H_z/\partial r\,\boldsymbol{\phi}]. \quad (30)$$

Using equations (21) and (30), the absorption pattern in the dielectric cylinder is obtained.

CALCULATIONS

Calculations are made for two circular triple-layered dielectric cylinder models: an arm size cylinder, and a thigh size cylinder. The arm size model has the dimensions $r_f = 4.45$ cm, $r_m = 3.175$ cm and $r_b = 0.95$ cm. The thigh size model has the dimensions $r_f = 8.9$ cm, $r_m = 6.35$ cm and $r_b = 1.9$ cm. Four frequencies are used in the calculation: 2450, 918, 750 and 433 MHz.

During the calculation, values of Bessel functions with complex arguments are required. The solutions of six by six complex matrix equations are also required. Using the method of series expansions taken from *Handbook of Mathematical Functions* (Ab64), the Bessel functions are calculated in a subroutine by the computer. The accuracy of the subroutine is checked against the values contained in the handbook. The accuracy is better than 10^{-8} within the range of the arguments and orders of the Bessel functions used in the heating pattern calculation. The inversion of the complex matrix is performed by the computer in another subroutine using the Gauss–Jordan Reduction Method (McC64).

Even though in this theoretical investigation, the original formulation is for triple-layered cylinders, the extension to arbitrary number of layers is easy. The algorithm of the computer program is such that it can be easily changed to accommodate the calculation of microwave absorption for tissue cylinders having any number of layers, subject to the limitation of the storage of the computer.

CONVERGENCE OF THE SERIES OF CYLINDRICAL WAVES

In order to ensure the convergence of the series of cylindrical waves for each frequency, an estimate is made for the values of the terms of the cylindrical waves as n, the number of terms, tends to infinity. The following asymptotic expressions for the Bessel functions can be used (Ho71).

$$J_n(z) \sim (1/\sqrt{2\pi n})(ez/2n)^n \quad (31)$$

$$Y_n(z) \sim -\sqrt{2/\pi n}\,(2n/ez)^n \quad (32)$$

$$H_n^{(2)}(z) \sim (1/\sqrt{2\pi n})[(ez/2n)^n + 2j(2n/ez)^n] \quad (33)$$

where $e = 2.71828\ldots$.

Consider equations (24) and (25). In order to determine the order of magnitude of A_{nf}, B_{nf} and C_n, each term of equation (24) is taken to have the same order of magnitude*. Hence, as a check for the order of magnitude of A_{nf}, B_{nf}, and C_n, the following expressions are used.

$$A_{nf}J_n(k_f r_f) \sim j^n J_n(k_0 r_f) \quad (34)$$

$$B_{nf}Y_n(k_f r_f) \sim j^n J_n(k_0 r_f) \quad (35)$$

$$C_n H_n^{(2)}(k_0 r_f) \sim j^n J_n(k_0 r_f). \quad (36)$$

Note that the above expressions can satisfy equation (25) if the asymptotic expressions for the Bessel functions are substituted into the equation. Substituting equations (31) through (33) into equations (34) through (36), the following expressions are obtained.

$$A_{nf} \sim (k_0/k_f)^n \quad (37)$$

$$B_{nf} \sim (e^2 k_0 k_f r_f^2/4n^2)^n \quad (38)$$

$$C_n \sim (e^2 k_0^2 r_f^2/4n^2)^n. \quad (39)$$

Putting the above approximations of the coefficients into the terms in the cylindrical wave, for $r_m \le r \le r_f$ (fat region)

$$A_{nf}J_n(k_f r) \sim (ek_0 r/2n)^n \quad (40)$$

$$B_{nf}Y_n(k_f r) \sim (ek_0 r_f^2/2nr)^n. \quad (41)$$

Hence the error for terminating the cylindrical wave at the N^{th} term is

$$\text{error} = \sum_{n=N}^{\infty} (ek_0 r_f^2/2nr)^n. \quad (42)$$

Note that the incident plane wave is defined to have an amplitude of 1. Hence the error is defined as the error relative to the amplitude of the incident plane wave.

For the muscle region, equations (26) and (27) are used. The same approximation procedures are again used. Hence, the following expressions for A_{nm} and B_{nm} are obtained.

$$A_{nm} \sim (k_0/k_m)^n (r_f/r_m)^{2n} \quad (43)$$

$$B_{nm} \sim (e^2 k_0 k_m r_f^2/4n^2)^n \quad (44)$$

$$A_{nm}J_n(k_m r) \sim (ek_0 r r_f^2/2nr_m^2)^n \quad (45)$$

$$B_{nm}Y_n(k_m r) \sim (ek_0 r_f^2/2nr)^n. \quad (46)$$

Hence the error term in the muscle region is the same as that of the fat region.

For the bone region,

$$A_{nb} \sim (k_0/k_b)^n (r_f/r_b)^{2n} \quad (47)$$

$$A_{nb}J_n(k_b r) \sim (ek_0 r r_f^2/2nr_b^2)^n. \quad (48)$$

The error term in the bone region is smaller than that of the fat and muscle regions.

Since k_0 depends on f, the higher frequency calculations require more terms for convergence than the lower frequency ones. Due to the dependence on r, the calculations for the thigh model require more terms than that of the arm model. Setting the error (relative to the amplitude of the incident plane wave) for truncation of the series at 10^{-3}, for the 2450 MHz thigh model case,

$$\sum_{n=N}^{\infty} (ek_0 r_f/2n)^n < 10^{-3}. \quad (49)$$

The value of N obtained is $N = 12$.

* These approximations are valid except for the case where $A_{nf}J_n(k_f r_f)$ and $B_{nf}Y_n(k_f r_f)$ are much larger than $j^n J_n(k_0 r_f)$, and that the sum of $A_{nf}J_n(k_f r_f)$ and $B_{nf}Y_n(k_f r_f)$ is such that equation (24) is satisfied. For this special case, the error checking is performed by the computer printout.

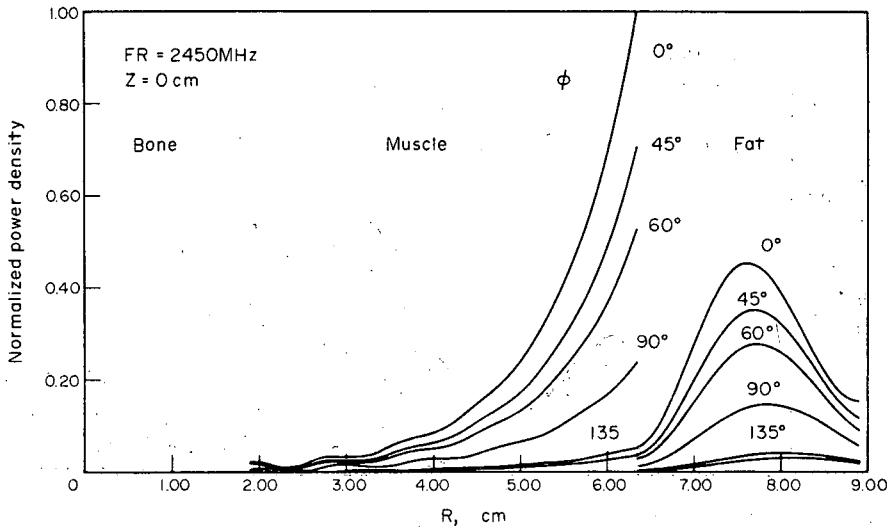

FIG. 2. Absorption patterns of thigh size model with plane wave source E_z polarization, freq. = 2450 MHz.

In the computer calculation, $N = 19$ is used for all cases. By comparing the results with the calculation for $N = 12$, the error is found to be well below 10^{-3}.

RESULTS

Figures 2–5 show the absorption patterns in a circular thigh size dielectric cylinder for incident E_z polarized (TM) plane waves of frequencies 2450, 918, 750 and 433 MHz respectively. Each of the absorbed power density (based on volume) patterns is normalized to its value in the muscle region at the fat–muscle interface. The reason for the choice of this normalization point is that for most of the cases investigated, the point of maximum absorption is in the muscle region at the fat–muscle interface.

In all cases, it is observed that the absorption is less intense in the fat region than in the

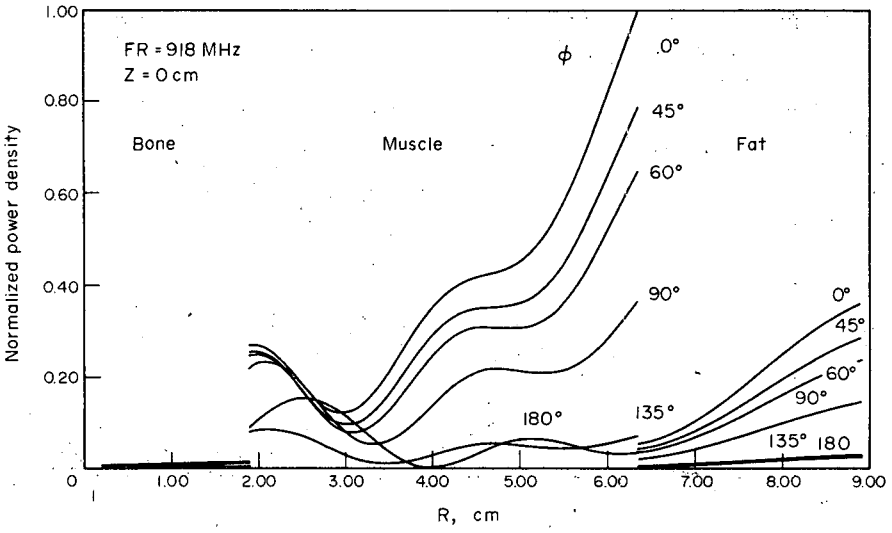

FIG. 3. Absorption patterns of thigh size model with plane wave source E_z polarization, freq. = 918 MHz.

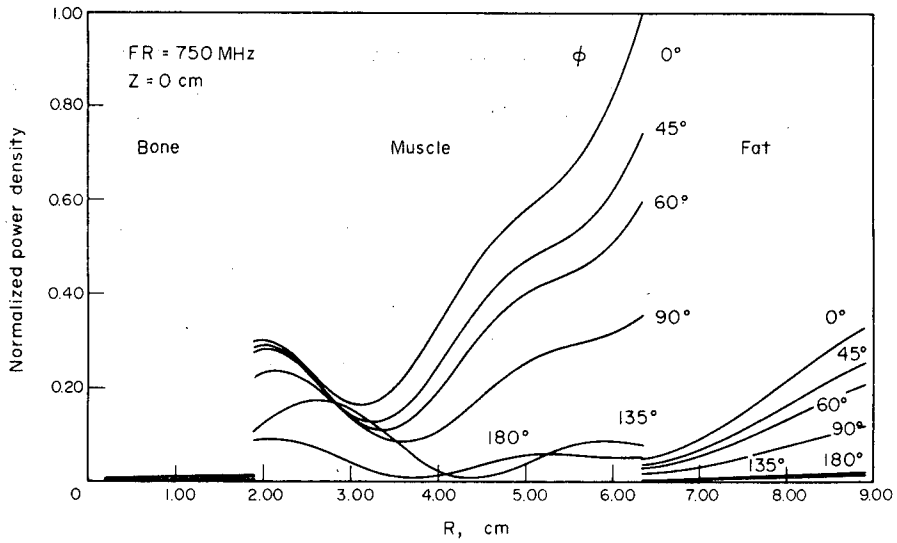

FIG. 4. Absorption patterns of thigh size model with plane wave source E_z polarization, freq. = 750 MHz.

muscle region. The bone region has practically no absorption at all. It is also observed that for the 2450 MHz case, the absorption in the muscle region attenuates almost exponentially from the fat–muscle interface. If the objective of therapeutic heating of human tissues with electromagnetic sources is to send heating deep into the muscle region, the penetration of heating into the muscle region for the 2450 MHz plane wave source is not very satisfactory. The decrease of frequency causes more penetration of heating into the muscle region and less heating in the fat region.

Figures 6–9 show the absorption patterns in a thigh size model due to H_z polarized (TE) plane wave sources. The general characteristics of the patterns are quite similar to that of the E_z polarized (TM) case. However, for the

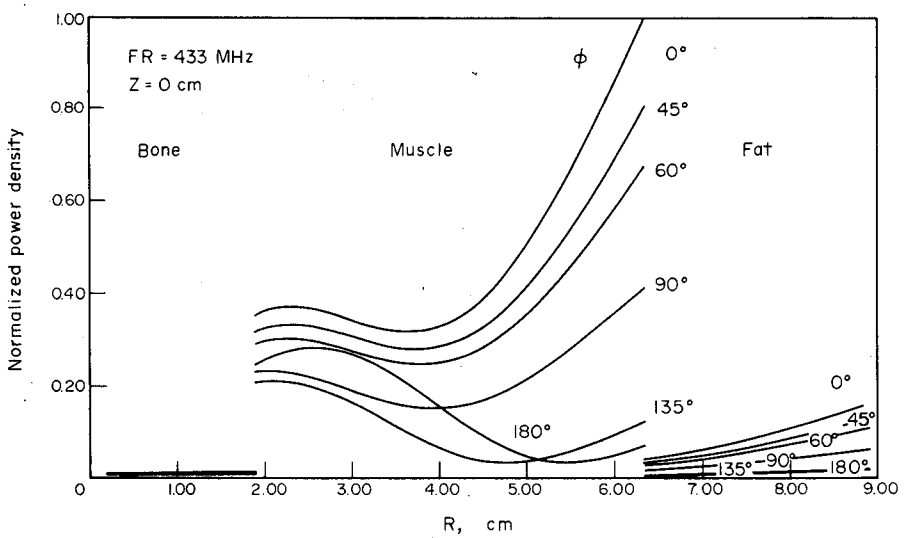

FIG. 5. Absorption patterns of thigh size model with plane wave source E_z polarization, freq. = 433 MHz.

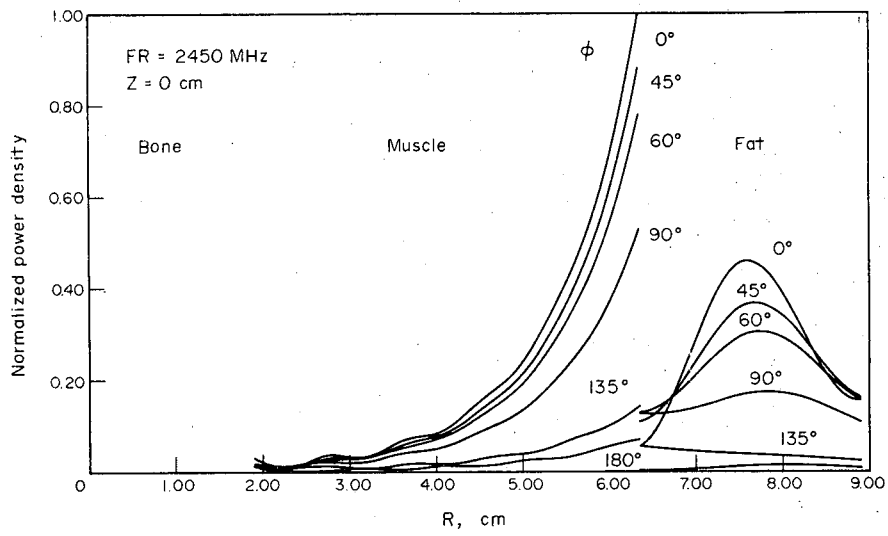

FIG. 6. Absorption patterns of thigh size model with plane wave source H_z polarization, freq. = 2450 MHz.

433 MHz case, there is a rather high intensity in the muscle region at the muscle–bone interface.

The absorption patterns in a circular arm size dielectric cylinder with incident E_z polarized (TM) plane wave sources are shown in Figs. 10–13. It is observed that in all cases the absorption in the bone region is negligible while the absorption in the fat region is smaller than that of the muscle region. The penetration of microwave energy in the muscle region is better than that of the thigh size model. Again the lowering of the frequency gives more even absorption in the muscle region and reduces the absorption in the fat region. Hence plane wave irradiation of the arm size model gives deeper penetration of energy into the muscle than for the case of the thigh

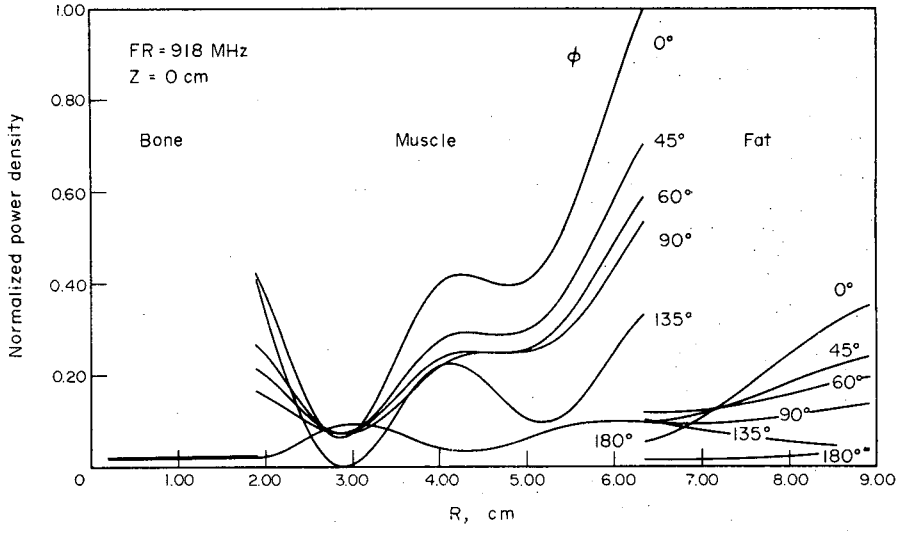

FIG. 7. Absorption patterns of thigh size model with plane wave source H_z polarization, freq. = 918 MHz.

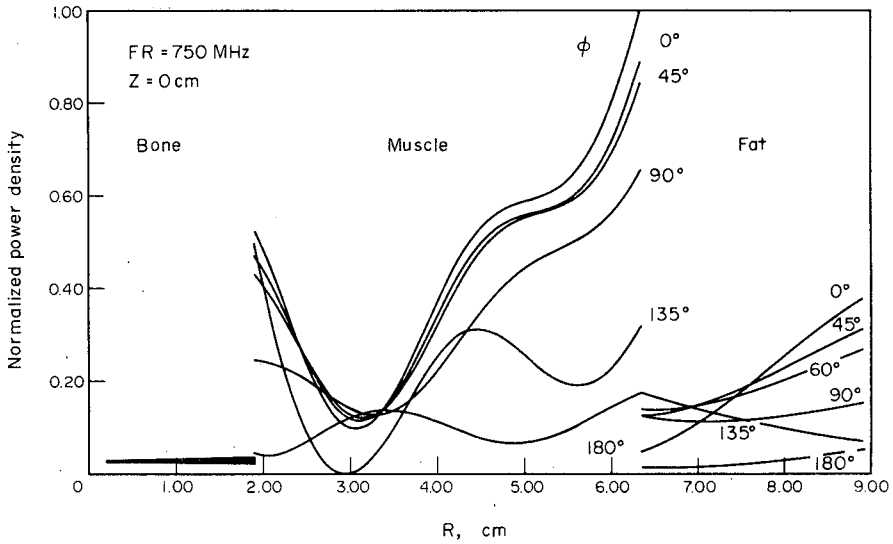

FIG. 8. Absorption patterns of thigh size model with plane wave source H_z polarization, freq. = 750 MHz.

model. Again the absorption characteristics of the 2450 MHz plane wave are inferior to those of the lower frequencies in terms of penetration of heating into the muscle region.

The heating patterns of the arm size model due to H_z polarized (TE) plane wave sources are shown in Figs. 14–17. The characteristics of the patterns are quite similar to that of the E_z polarized (TM) case. However, in the H_z polarized (TE) case, the absorption in the muscle region is more intense at the muscle–bone interface than at the fat–muscle interface. This deep penetration of energy into the muscle region may be beneficial in terms of therapeutic heating of human tissues.

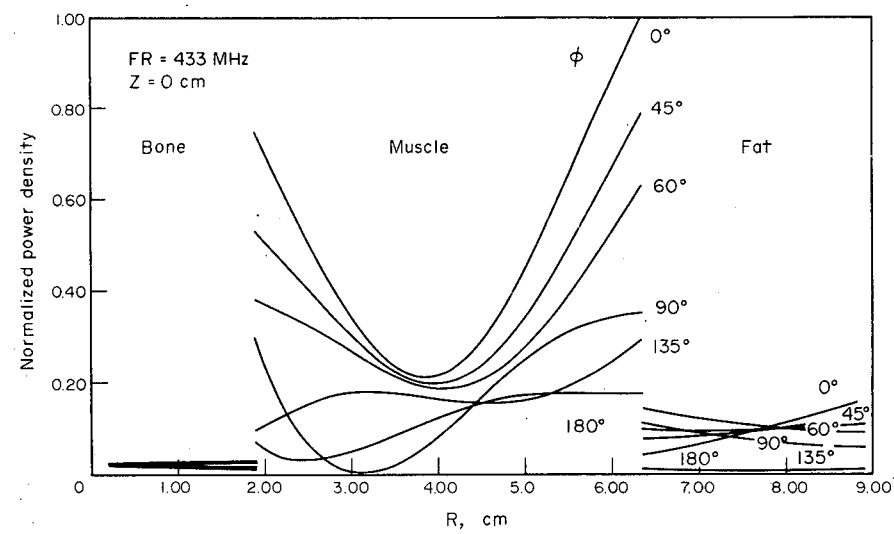

FIG. 9. Absorption patterns of thigh size model with plane wave source H_z polarization, freq. = 433 MHz.

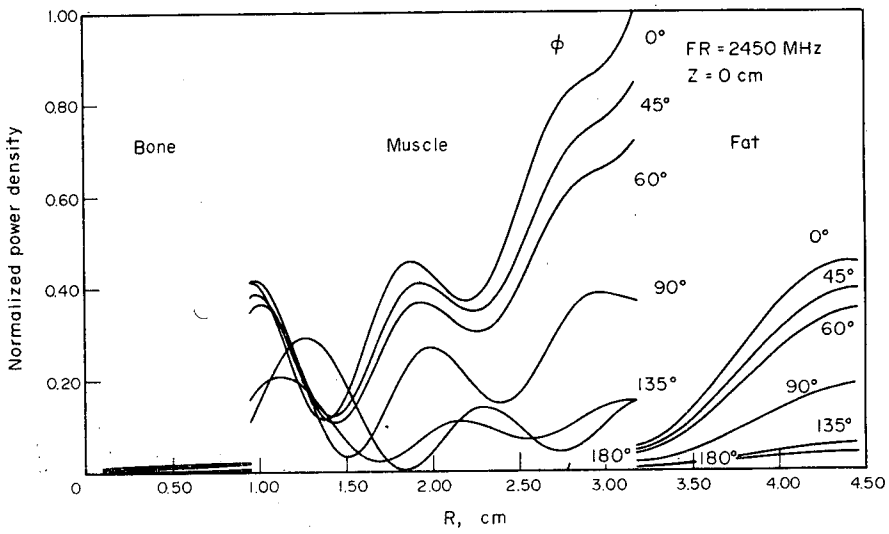

FIG. 10. Absorption patterns of arm size model with plane wave source E_z polarization, freq. = 2450 MHz.

CONCLUSIONS

This theoretical investigation shows the large variation of energy absorption characteristics in tissues for different source frequencies and sizes of biological bodies. It is therefore important to recognize these microwave characteristics in the design and the interpretation of the results of biological effects experiments in relation to health protection. The limitations of the usefulness of incident power density in biological experiments using animals of various sizes is evident. It is recommended that dosimetry in biological effects experiments be quantified in terms of total absorbed energy and the distribution of the absorbed energy in the biological body. Additionally, the determinations of the absorption

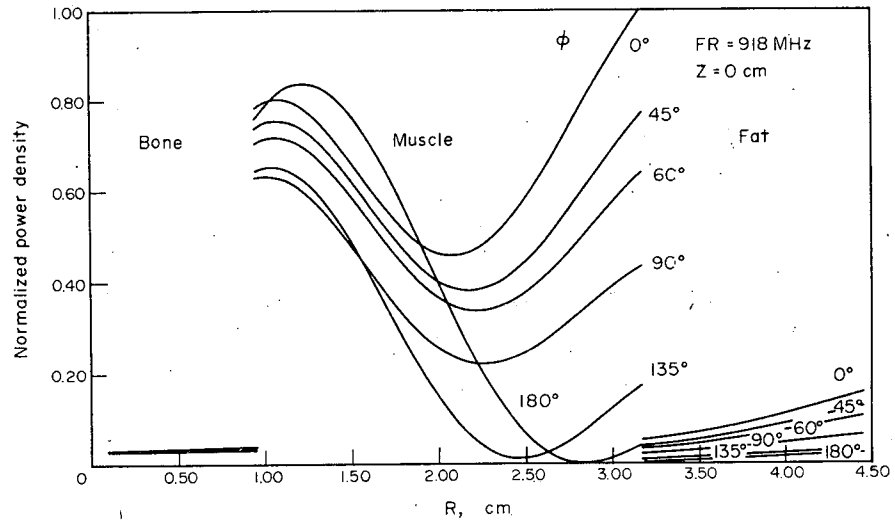

FIG. 11. Absorption patterns of arm size model with plane wave source E_z polarization, freq. = 918 MHz.

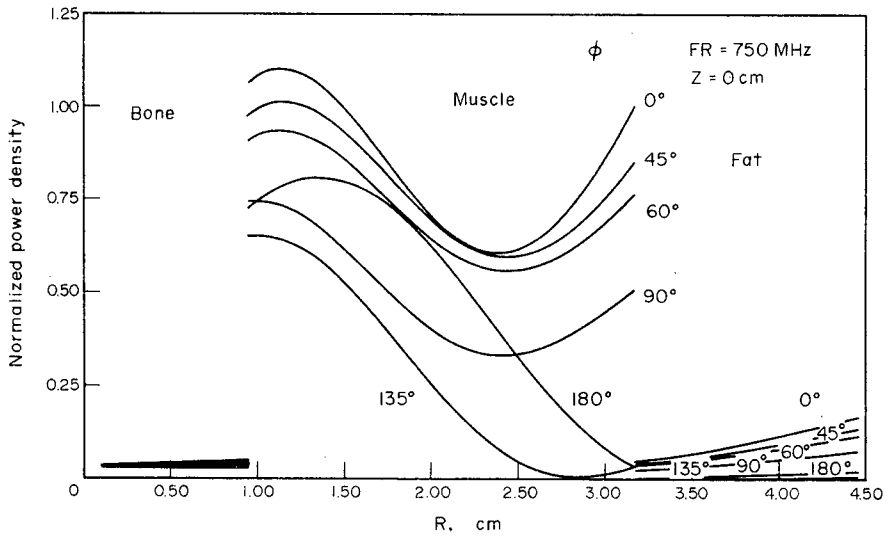

FIG. 12. Absorption patterns of arm size model with plane wave source E_z polarization, freq. = 750 MHz.

characteristics of phantom human bodies are needed for given exposures to microwave radiations.

This investigation also shows the many possible patterns of energy deposition in tissues that can be achieved with varying tissue sizes and source frequencies. Research on the absorption characteristics in models of tissues exposed to aperture sources has been previously reported (Ho71; Ho75). Additional research is needed for the practical design of effective applicators.

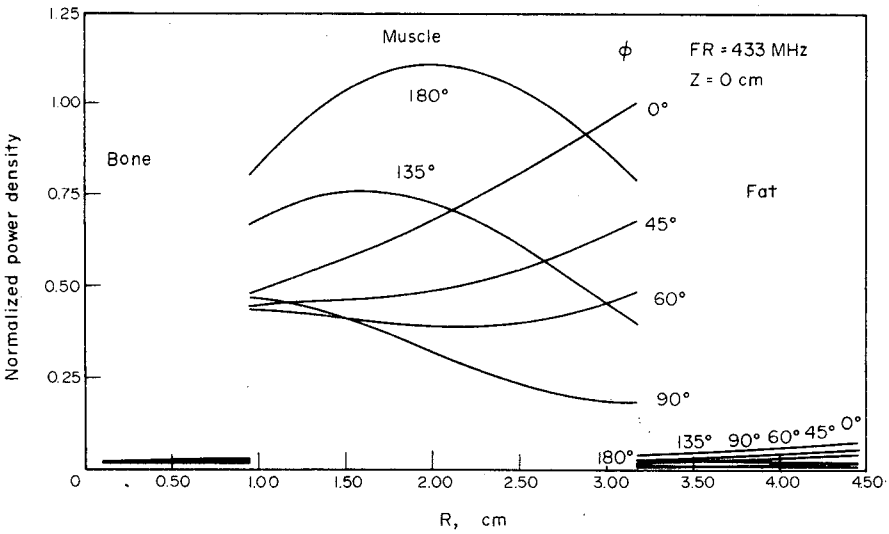

FIG. 13. Absorption patterns of arm size model with plane wave source E_z polarization, freq. = 433 MHz.

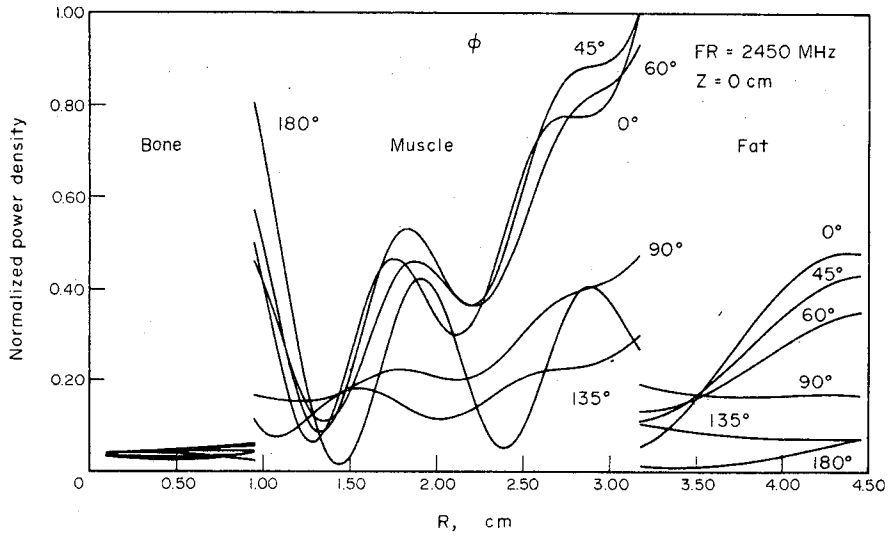

FIG. 14. Absorption patterns of arm size model with plane wave source H_z polarization, freq. = 2450 MHz.

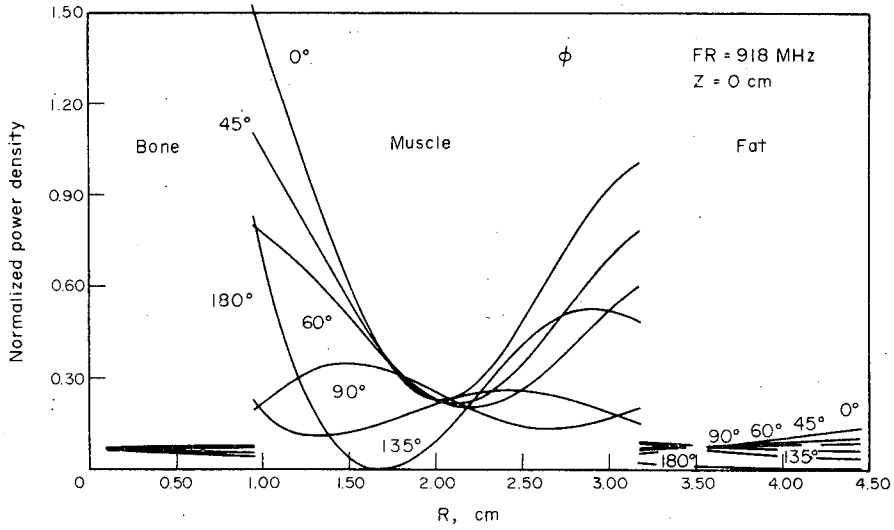

FIG. 15. Absorption patterns of arm size model with plane wave source H_z polarization, freq. = 918 MHz.

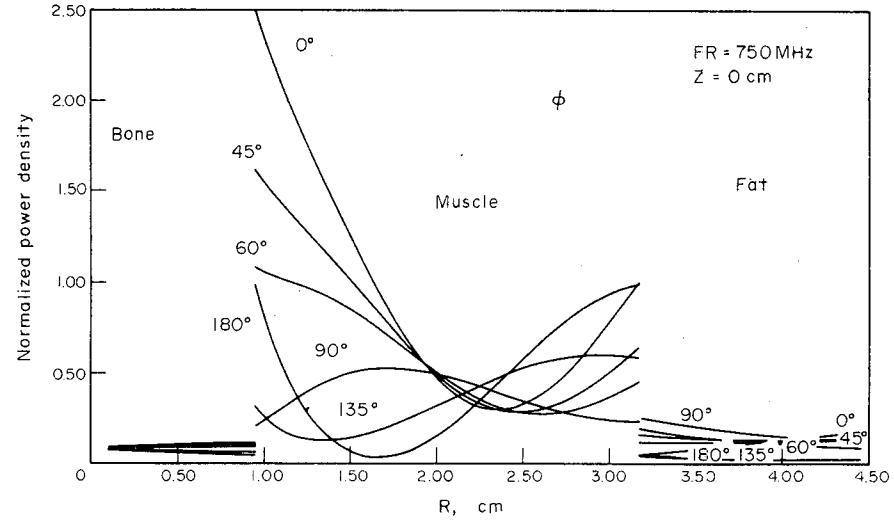

FIG. 16. Absorption patterns of arm size model with plane wave source H_z polarization, freq. = 750 MHz.

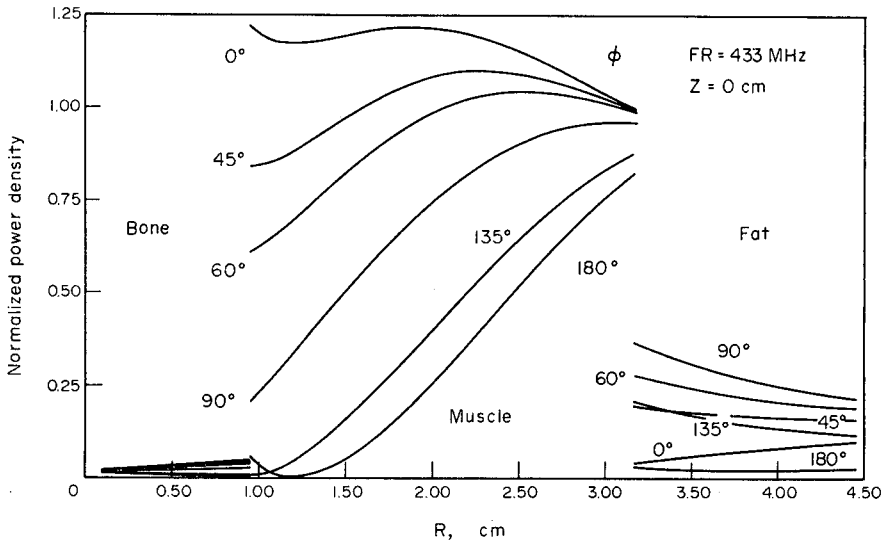

FIG. 17. Absorption patterns of arm size model with plane wave source H_z polarization, freq. = 433 MHz.

Acknowledgement—This investigation was performed by the author at the University of Washington, supported in part by Social Rehabilitation Service Research and Training Grant 16-P-56818/0-09 and Bureau of Radiological Health Grant 8-R01-RL00528-02.

REFERENCES

Ab64 Abramowitz M. and Stegun I. A., 1964, *Handbook of Mathematical Functions*, pp. 355–433. National Bureau of Standards.

Ho71 Ho H. S., Guy A. W., Sigelmann R. A., and Lehmann J. F., 1971, *Microwave Heating of Simulated Human Limb by Aperture Sources*, IEEE Trans. on Microwave Theory and Tech., Vol. MTT-19, No. 2, pp. 224–231.

Ho75 Ho H. S., 1975, "Contrast of Dose Distribution in Phantom Heads due to Aperture and Plane Wave Sources," *Annls N.Y. Acad. Sci.* **247,** 454.

Jo73 Johnson C. C., 1973, "Research Needs for Establishing a Radio Frequency Electromagnetic Radiation Safety Standard," J. *Microwave Power* **8** (Nos. 3 & 4), 370.

McC64 McCormick J. M. and Salvadori M. G., 1964, *Numerical Methods in FORTRAN* (Englewood Cliffs, N.J.: Prentice-Hall).

Sc54 Schwan H. P. and Piersol G. M., 1954, "The absorption of Electromagnetic Energy in Body Tissues," *Am. J. Phys. Med.* **33,** 370.

Wo55 Wait J. R., 1955, "Scattering of a Plane Wave from a Circular Dielectric Cylinder at Oblique Incidence," *Can. J. Phys.* **33,** 189.